A Shallow Cumuliform Snowfall Census Using Spaceborne Radar

MARK S. KULIE, LISA MILANI, NORMAN B. WOOD, SAMANTHA A. TUSHAUS, AND RALF BENNARTZ

Space Science and Engineering Center, University of Wisconsin–Madison, Madison, Wisconsin

TRISTAN S. L'ECUYER

Space Science and Engineering Center, and Department of Atmospheric and Oceanic Sciences, University of Wisconsin–Madison, Madison, Wisconsin

(Manuscript received 22 July 2015, in final form 9 February 2016)

ABSTRACT

The first observationally based near-global shallow cumuliform snowfall census is undertaken using multiyear *CloudSat* Cloud Profiling Radar observations. *CloudSat* snowfall observations and snowfall rate estimates from the *CloudSat* 2C-Snow Water Content and Snowfall Rate (2C-SNOW-PROFILE) product are partitioned between shallow cumuliform and nimbostratus cloud structures by utilizing coincident cloud category classifications from the *CloudSat* 2B-Cloud Scenario Classification (2B-CLDCLASS) product. Shallow cumuliform (nimbostratus) snowfall events comprise about 36% (59%) of snowfall events in the *CloudSat* snowfall dataset. The remaining 5% of snowfall events are distributed between other categories. Distinct oceanic versus continental trends exist between the two major snowfall categories, as shallow cumuliform snow-producing clouds occur predominantly over the oceans. Regional differences are also noted in the partitioned dataset, with over-ocean regions near Greenland, the far North Atlantic Ocean, the Barents Sea, the western Pacific Ocean, the southern Bering Sea, and the Southern Hemispheric pan-oceanic region containing distinct shallow snowfall occurrence maxima exceeding 60%. Certain Northern Hemispheric continental regions also experience frequent shallow cumuliform snowfall events (e.g., inland Russia), as well as some mountainous regions. *CloudSat*-generated snowfall rates are also partitioned between the two major snowfall categories to illustrate the importance of shallow snow-producing cloud structures to the average annual snowfall. While shallow cumuliform snowfall produces over 50% of the annual estimated surface snowfall flux regionally, about 18% (82%) of global snowfall is attributed to shallow (nimbostratus) snowfall. This foundational spaceborne snowfall study will be utilized for follow-on evaluative studies with independent model, reanalysis, and ground-based observational datasets to characterize respective dataset biases and to better quantify *CloudSat* snowfall detection and quantitative snowfall estimate uncertainties.

1. Introduction

Accumulating surface snowfall is generated from cloud structures with varying vertical extent and underlying formation mechanisms. For instance, midlatitude winter cyclones with complex dynamical forcing produce snowfall from incipient cloud structures typically extending into the mid- to upper troposphere. Common examples of snowfall events associated with deeper clouds in the continental North American region include U.S. East Coast winter storms (e.g., Kocin and Uccellini 1990), lee cyclogenesis events in the U.S. Great Plains (e.g., Rauber et al. 2014), and fast-moving "Alberta clipper" systems that originate on the lee side of the Canadian Rocky Mountain system and produce snowfall across much of central and eastern North America (e.g., Thomas and Martin 2007; Plummer et al. 2014). Alternatively, snowfall produced by shallow clouds—where "shallow" is generically defined as lower-tropospheric cloud-top heights—commonly occurs in many locations, especially near larger bodies of water in the mid- and high latitudes. Lake-effect snow is a well-documented form of shallow cumuliform snowfall resulting from cold-air outbreaks in the wake of midlatitude cyclones that interact with unfrozen or partially frozen bodies of water

Corresponding author address: Mark S. Kulie, Space Science and Engineering Center, University of Wisconsin–Madison, 1225 W. Dayton St., Madison, WI 53706.
E-mail: mskulie@wisc.edu

DOI: 10.1175/JHM-D-15-0123.1

(e.g., Holroyd 1971; Niziol 1987; Kristovich and Steve 1995; Kristovich and Laird 1998). Lake-effect snow is responsible for enhanced annual snowfall totals throughout much of the United States and Canadian Great Lakes region (Scott and Huff 1996; Notaro et al. 2013) and is therefore an integral component of the Great Lakes hydrologic budget. Lake-effect snow also impacts regional ecology (Henne et al. 2007; Kolka et al. 2010) and exerts substantial socioeconomic effects in the Great Lakes basin (e.g., Changnon 1979; Schmidlin et al. 1992; Norton and Bolsenga 1993; Schmidlin 1993; Kunkel et al. 2002).

While ground-based observations of shallow snowfall are plentiful in certain locations like the Great Lakes region, shallow snowfall has also been documented in observational studies from other locations near large bodies of water such as the Great Salt Lake (e.g., Schultz 1999; Steenburgh et al. 2000; Yeager et al. 2013), the Sea of Japan–Okhotsk region (Katsumata et al. 2000; Noh et al. 2006), the Baltic Sea–Gulf of Finland region (e.g., Andersson and Nilsson 1990; Mazon et al. 2015), and the Irish Sea (Norris et al. 2013). Bech et al. (2013) also studied a thundersnow event associated with relatively shallow cloud features in Spain near the Mediterranean Sea. Smaller inland lakes such as the Finger Lakes region in upstate New York also produce appreciable lake-effect snow (Laird et al. 2010). Lake-effect snow, however, is not the only form of shallow snowfall. Shallow Arctic clouds, with forcing mechanisms that differ from lake-effect snow, also commonly produce snowfall. Snow-generating Arctic mixed-phase clouds are also an important supercooled cloud liquid water sink that alters the radiative effects of such clouds (e.g., Shupe et al. 2006, 2013). Airborne radar observations have also indicated orographically induced mountain snowfall originating from fairly shallow cloud structures above ground level (Pokharel et al. 2014; Geerts et al. 2015).

Shallow snowfall occurs pervasively around the world because of a handful of possible mechanisms, but a truly global observational accounting of shallow snowfall has not been undertaken because of the dearth of active ground-based observations capable of providing global snowfall information. Furthermore, available operational ground-based radars struggle to detect shallow snowfall events at distances greater than ~100–150 km from the radar sites because of the lowest elevation angle scan overshooting shallow snowfall structures. Therefore, the main purpose of this study is to compile a multiyear near-global[1] census of shallow snowfall from an active spaceborne remote sensing perspective using *CloudSat* observations, with overwater snowfall production that is particularly inaccessible to ground-based radars being the primary motivating factor to undertake this study.

CloudSat (Stephens et al. 2002) carries the W-band (94 GHz) Cloud Profiling Radar (CPR; Tanelli et al. 2008) that has collected data since its 2006 launch. While *CloudSat* was designed as primarily a cloud remote sensing mission, its high-latitude coverage (up to ~|82°| latitude) and high radar sensitivity (~−28 dBZ) make it very suitable for snowfall-related research. Numerous recent investigations have highlighted *CloudSat*'s importance to the snowfall remote sensing community, both in proof-of-concept studies comparing *CloudSat* observations and snowfall rate retrievals with ground-based radar observations (e.g., Hudak et al. 2008; Matrosov et al. 2008) and for studies using extended *CloudSat* observations to assess global snowfall distribution and to quantify uncertainties related to single-frequency, W-band snowfall retrievals (e.g., Liu 2008; Kulie and Bennartz 2009; Hiley et al. 2011; Wang et al. 2013; Behrangi et al. 2014). Additional recent studies have focused on *CloudSat* snowfall estimates in specific high-interest locations like Antarctica to assess *CloudSat* snowfall retrievals with independent remote sensing, reanalysis and ground-based datasets (Boening et al. 2012; Palerme et al. 2014; Milani et al. 2015).

This investigation's shallow snowfall focus builds on previous global spaceborne radar studies of shallow rainfall. Investigators have utilized Tropical Rainfall Measuring Mission (Simpson et al. 1988; Kummerow et al. 1998) Precipitation Radar observations to characterize shallow, tropical precipitation occurrence and global rain fraction (e.g., Short and Nakamura 2000; Schumacher and Houze 2003; Liu and Zipser 2009). *CloudSat* observations have also been used for shallow rainfall retrievals, especially associated with marine stratocumulus clouds (e.g., Lebsock and L'Ecuyer 2011; Lebsock et al. 2011; Rapp et al. 2013). *CloudSat*'s ability to detect shallow snowfall has been highlighted in recent studies. Liu (2008) indicated both oceanic and land shallow snowfall modes when analyzing dominant mean reflectivity profiles associated with *CloudSat*-indicated snowfall events [e.g., see Fig. 11 in Liu (2008)]. Liu (2008) also noted intense snowfall rates associated with shallow radar reflectivity profiles and suggested lake-effect snow as the most likely mechanism to explain this trend. Kulie and Bennartz (2009) also discussed a globally significant shallow snowfall mode when illustrating the sensitivity of a vertical continuity reflectivity threshold created to mitigate potential ground clutter contamination over land. The ad hoc vertical continuity

[1] "Near global" and "global" are used interchangeably throughout the text when discussing *CloudSat* observations, where "global" is understood to represent the latitudinal coverage of *CloudSat* between ~|82°|.

criterion used in Kulie and Bennartz (2009) required the lowest five contiguous CPR observations to exceed a minimum reflectivity threshold in order to be classified as a likely surface snowfall event. The vertical continuity requirement was shown to greatly reduce the occurrence of clutter-infected observations in isolated regions (e.g., Greenland's coastline), but probably at the expense of removing legitimate shallow snowfall cases from the *CloudSat* snowfall event database in other locales. In fact, Hiley et al. (2011) demonstrated that relaxing or eliminating the suggested vertical continuity requirement in Kulie and Bennartz (2009), especially over ocean where elevated ground clutter is not prevalent, greatly increased the number of snowfall observations contained in the *CloudSat* snowfall dataset and thus reflected an ubiquitous shallow snowfall mode in many oceanic regions. Certain continental regions were also sensitive to these tests, especially over the interior of Russia, thus suggesting frequent shallow snowfall events over land. Finally, Wang et al. (2013) used a multiyear coincident *CloudSat* and passive microwave radiometer dataset to study cloud liquid water in snowfall events. The Wang et al. (2013) study partitioned snowfall events into various snowfall categories based on *CloudSat*-estimated cloud-top height to illustrate the distribution of cloud liquid water by snowfall type and the multifrequency microwave radiometer response to cloud liquid water. Further methodological differences between the Wang et al. (2013) study and the current study are discussed in section 2. While these previous studies introduced *CloudSat*'s ability to detect shallow snowfall, a multiyear shallow snowfall analysis to elucidate the spatial distribution of shallow snowfall and its estimated contribution to annual snowfall is currently lacking on a global scale.

A shallow snowfall census is further motivated by the recent launch of the Global Precipitation Measurement (GPM) mission (Hou et al. 2014). GPM and its constellation satellites utilize passive microwave radiometers that have produced a rich legacy of global precipitation retrievals (e.g., Huffman et al. 2001, 2007, 2009). Shallow snowfall is a unique precipitation mode emanating from cloud structures associated with potentially unique microphysical composition and radiometric signatures (Noh et al. 2006; Wang et al. 2013), so developing a database of shallow snowfall events concurrent with microwave radiometer observations is crucial to develop and evaluate GPM snowfall retrievals. Combined *CloudSat* and Advanced Microwave Scanning Radiometer for Earth Observing System (AMSR-E) observations from the so-called afternoon constellation, or A-Train, can be leveraged for such purposes (e.g., Kulie et al. 2010; Wang et al. 2013). In fact, a database of *CloudSat* and AMSR-E observations is used in the at-launch operational version of GPM snowfall retrievals for cold surfaces at high latitudes (Kummerow et al. 2015). Further motivation to develop a shallow snowfall data record is also provided by recent studies that predict shallow lake-effect snowfall events may be significantly altered by a warming climate at higher latitudes (e.g., Burnett et al. 2003; Kunkel et al. 2009; Notaro et al. 2014). Recent research using model output has also posited that future Arctic precipitation may substantially increase, largely driven by local surface evaporation effects—the prime mechanism causing overwater shallow snowfall—due to diminished sea ice coverage (Bintanja and Selten 2014). The *CloudSat* data record serves as a valuable reference to monitor future changes in shallow snowfall frequency and location, especially if long-term active spaceborne observations capable of observing shallow snowfall follow *CloudSat*.

This study will therefore explore shallow snowfall from a spaceborne remote sensing perspective. The following key questions will be addressed in this investigation:

- Can *CloudSat* observations and data products successfully partition snowfall to produce a near-global snowfall census separated by different snowfall modes (e.g., shallow cumuliform vs nimbostratus snowfall-producing cloud structures)?
- Where does shallow cumuliform snowfall preferentially occur and is it the predominant snowfall mode anywhere? Do distinct land versus ocean shallow snowfall signatures exist in the dataset?
- How much does shallow snowfall typically contribute to the total annual snowfall accumulation both globally and regionally?

A description of the data and methods used in this study is provided in section 2, while section 3 provides an overview of global snowfall partitioned between different snowfall modes. Section 4 provides a summary and discussion, including future research pathways related to this study.

2. Data and methods

a. CloudSat *product description*

CloudSat CPR observations and affiliated products are the primary data sources used in this study. The CPR is a near-nadir-pointing, nonscanning radar with a mean spatial resolution of ~1.4 (cross track) × ~1.8 km (along track) and produces vertical radar reflectivity factor (hereafter referred to as "radar reflectivity" or "reflectivity" for brevity) profiles with 240-m grid spacing in the *CloudSat* data products. The following level 2 products

TABLE 1. *CloudSat* products and parameters used in this study from each respective product.

CloudSat product	Field
2B-GEOPROF	Radar reflectivity factor, land–sea flag, elevation, latitude, and longitude
ECMWF-AUX	Temperature profiles
2C-SNOW-PROFILE	Near-surface snowfall rate
2B-CLDCLASS	Cloud classification
2C-PRECIP-COLUMN	Surface type, sea surface temperature, and cloud-top height for lowest significant cloud layer

(release R04) are used in this study: 2B-Geometric Profile (2B-GEOPROF), 2C-Snow Water Content and Snowfall Rate (2C-SNOW-PROFILE), 2B-Cloud Scenario Classification (2B-CLDCLASS), 2C-Precipitation Column (2C-PRECIP-COLUMN), and European Centre for Medium-Range Weather Forecasts–Auxiliary (ECMWF-AUX). The aforementioned products are orbital swath products distributed by the *CloudSat* Data Processing Center. A *CloudSat* data record from June 2006 through December 2010 (*CloudSat* epochs 00–02) is utilized for this study. *CloudSat* observations are available from 2011 to present, but a battery anomaly in 2011 created a multimonth data gap and necessitated the transition to a sunlight-only operational mode. The 2006–10 data period also aligns with near-coincident AMSR-E observations that will be used in future synergistic studies (AMSR-E ceased operations in 2011).

Table 1 summarizes the various fields obtained from each data product that are used in this investigation. Radar reflectivity profiles, as well as digital elevation maps, are obtained from the 2B-GEOPROF product. The 2C-PRECIP-COLUMN product is primarily a surface rainfall product, but surface type classifications, sea surface temperatures, and cloud-top heights of the lowest significant cloud structure in the observational column are employed in this study. Temperature profiles and other atmospheric state variables (e.g., water vapor content and pressure) are obtained from the ECMWF-AUX product that interpolates ECMWF model data to each *CloudSat* observation.

The two most important retrieved quantities used in this study are near-surface snowfall rates and cloud classifications obtained from the 2C-SNOW-PROFILE and 2B-CLDCLASS products, respectively. The 2C-SNOW-PROFILE product retrieves snowfall rates from the CPR reflectivity observations via an optimal estimation approach to derive dynamic radar reflectivity Z_e to snowfall rate S relationships (Wood et al. 2013). The 2C-SNOW-PROFILE algorithm leverages the 2C-PRECIP-COLUMN product and automatically generates snowfall rate estimates when 2C-PRECIP-COLUMN indicates near-surface "snow possible" or "snow certain" conditions [e.g., see Haynes et al. (2009), (2013) for further details]. The near-surface bin is defined as the third (fifth) range bin above the declared surface bin over oceanic (land) surfaces. Both 2C-SNOW-PROFILE and 2C-PRECIP-COLUMN utilize the cloud mask field contained in the 2B-GEOPROF product and only consider CPR observations associated with a cloud mask equal to or exceeding 20, where cloud mask values of 20, 30, and 40 are labeled "weak echo," "good echo," and "strong echo" and are associated with false detection rates of ~5%, 4%, and 1% when compared against *Cloud–Aerosol Lidar and Infrared Pathfinder Satellite Observations* (*CALIPSO*) lidar observations, respectively (Marchand et al. 2008). If 2C-PRECIP-COLUMN flags near-surface observations as "mixed possible" or "mixed certain," the 2C-SNOW-PROFILE algorithm produces a snowfall rate estimate only if the estimated melted fraction from the 2C-PRECIP-COLUMN product is less than or equal to 0.1. If the 2C-PRECIP-COLUMN precipitation phase indicators are unclear or melted fraction is not provided, the 2C-SNOW-PROFILE algorithm uses a snow discrimination algorithm based on ECMWF-AUX surface temperature, an assumed lapse rate, and an idealized melting model. The internal 2C-SNOW-PROFILE phase algorithm allows a 240-m layer depth for snow to significantly melt. This assumed melting layer depth enables snowfall retrievals to be made for surface temperatures up to ~1.5°C. The 2C-SNOW-PROFILE optimal estimation scheme is constrained by a priori snow microphysical properties (e.g., observed mass–size relationships and particle size distributions collected during field campaigns, plus modeled backscatter properties of nonspherical frozen hydrometeors) and provides snow size distribution parameter and snowfall rate uncertainty estimates combined with snowfall rate retrievals (Wood et al. 2014, 2015). Ground clutter is also partially mitigated by taking advantage of the 2C-SNOW-PROFILE snow retrieval status (SRS) flag that highlights CPR snowfall retrievals associated with a strong vertical radar reflectivity gradient in the lowest bins. Observations associated with strong vertical reflectivity or snowfall rate gradients might be indicative of ground clutter. Global maps of this flag (not shown) systematically indicate ground clutter in a few select locations (e.g., Antarctica and Greenland), so snowfall rate retrievals from higher in the column are utilized to alleviate potentially clutter-infected observations [see Milani et al. (2015) for further details].

The 2B-CLDCLASS product is used to discriminate shallow cumuliform (e.g., stratocumulus or cumulus) versus precipitating stratiform (e.g., nimbostratus) snow-producing

cloud structures. The 2B-CLDCLASS cloud classification algorithm uses space-based active (*CloudSat* CPR and *CALIPSO*) and passive [Moderate Resolution Imaging Spectroradiometer (MODIS)] remote sensing observations to identify cloud properties such as vertical and horizontal cloud extent, precipitation occurrence, cloud temperature and maximum reflectivity, and upward radiance [see Wang and Sassen (2007) and Sassen and Wang (2008) for further theoretical framework]. This information allows cloud structures to be classified as cumulus, stratocumulus, stratus, nimbostratus, alto-type clouds, deep convective, and cirrus. While the algorithm takes into account cloud features (cloud base, precipitation production, size, etc.) previously quantified in the literature, it also uses the more complex *CloudSat* data to craft a decision tree. The algorithm first identifies cloud layers or clusters. It then determines if clouds are precipitating, using measured precipitation and cloud-top height. Using maximum reflectivity, the height at which it occurs, and the cloud base and top, the algorithm then distinguishes between high and low clouds.

b. *Snowfall partitioning methodology and examples*

Nonzero, near-surface 2C-SNOW-PROFILE snowfall retrievals are partitioned into a shallow cumuliform (‘‘shallow’’ is hereafter often used for brevity) snowfall dataset using coincident 2B-CLDCLASS ‘‘stratocumulus’’ and ‘‘cumulus’’ cloud classifications. Near-surface snow observations from all other 2B-CLDCLASS cloud categories are retained, with ‘‘nimbostratus’’ clouds serving as the second important snowfall category analyzed in this study. Snowfall occurrences coincident with other cloud-type retrievals will be briefly discussed even though they comprise only a small percentage of the *CloudSat* snowfall database.

As defined by the stratocumulus and cumulus cloud categories, shallow convective snow-producing clouds are usually linked with boundary layer processes (lake-effect snow, overland boundary layer rolls, etc.), while the nimbostratus designation is associated with horizontally contiguous reflectivity structures that are typically, but not universally, thicker than shallow cumuliform clouds. The 2C-PRECIP-COLUMN lowest significant cloud-layer height in the column is used to define the snow-producing cloud structure thickness for each *CloudSat* snowfall observation (‘‘snowfall’’ or ‘‘snowfall observation’’ is hereafter applied to *CloudSat*-detected snowfall events that have a valid reflectivity and snowfall rate retrieval in the designated near-surface bin). The lowest significant cloud-layer height (‘‘cloud thickness’’ for brevity) above ground/ocean level (AGL) is used rather than the absolute maximum reflectivity-defined cloud-top height to avoid misclassification due to multilevel cloud structures. Figure 1 illustrates the distinct cloud thickness distributions for the shallow and nimbostratus snowfall categories based on 2B-CLDCLASS classifications. The shallow snowfall normalized cloud thickness distribution peaks between ~1 and 2 km and exhibits a very narrow distribution. Almost 89% of all cumuliform snow-producing clouds are associated with cloud thicknesses less than 3 km, thus serving as justification to apply the ‘‘shallow’’ qualifier to such snow-producing clouds. Conversely, the nimbostratus normalized cloud thickness distribution is much broader and centered near 4–5 km. While over 77% of nimbostratus clouds exceed the 3-km cloud thickness threshold, the nimbostratus cloud thickness distribution overlaps the cumuliform/shallow category in the sub-3-km range, thus indicating a mode of nimbostratus snowfall-producing cloud that does not possess extensive vertical development. Cloud thickness is therefore not an exclusive discriminant between the two primary snow categories, but the nimbostratus category is more likely to be associated with deeper cloud structures than the cumuliform category.

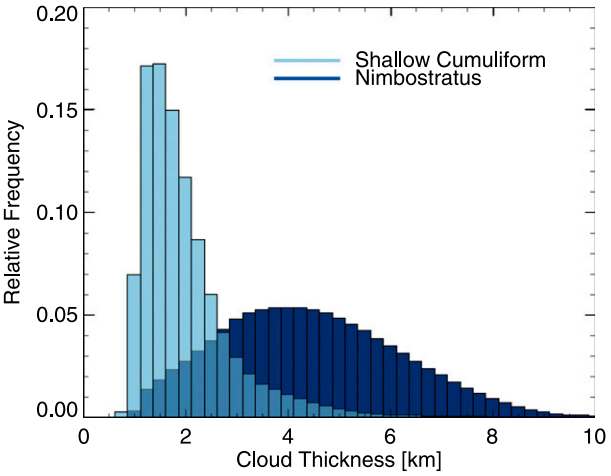

FIG. 1. Cloud-top thickness distributions associated with shallow cumuliform (light blue) and nimbostratus (dark blue) *CloudSat* snowfall-producing cloud structures. A 250-m cloud thickness bin size is used to construct the distributions. Shallow vs deeper nimbostratus snowfall categories are defined by the *CloudSat* 2B-CLDCLASS product, while cloud thicknesses are calculated from the 2B-GEOPROF and 2C-PRECIP-COLUMN products (see text for details).

The snowfall partitioning scheme adopted in this study is not the first published attempt at categorizing *CloudSat* snowfall events based into shallow versus deeper structures. Wang et al. (2013) presented a partitioning methodology to discriminate shallow versus deeper snowfall events using *CloudSat* reflectivity characteristics. Wang et al. (2013) classified shallow snowfall events with *CloudSat*-estimated cloud-top

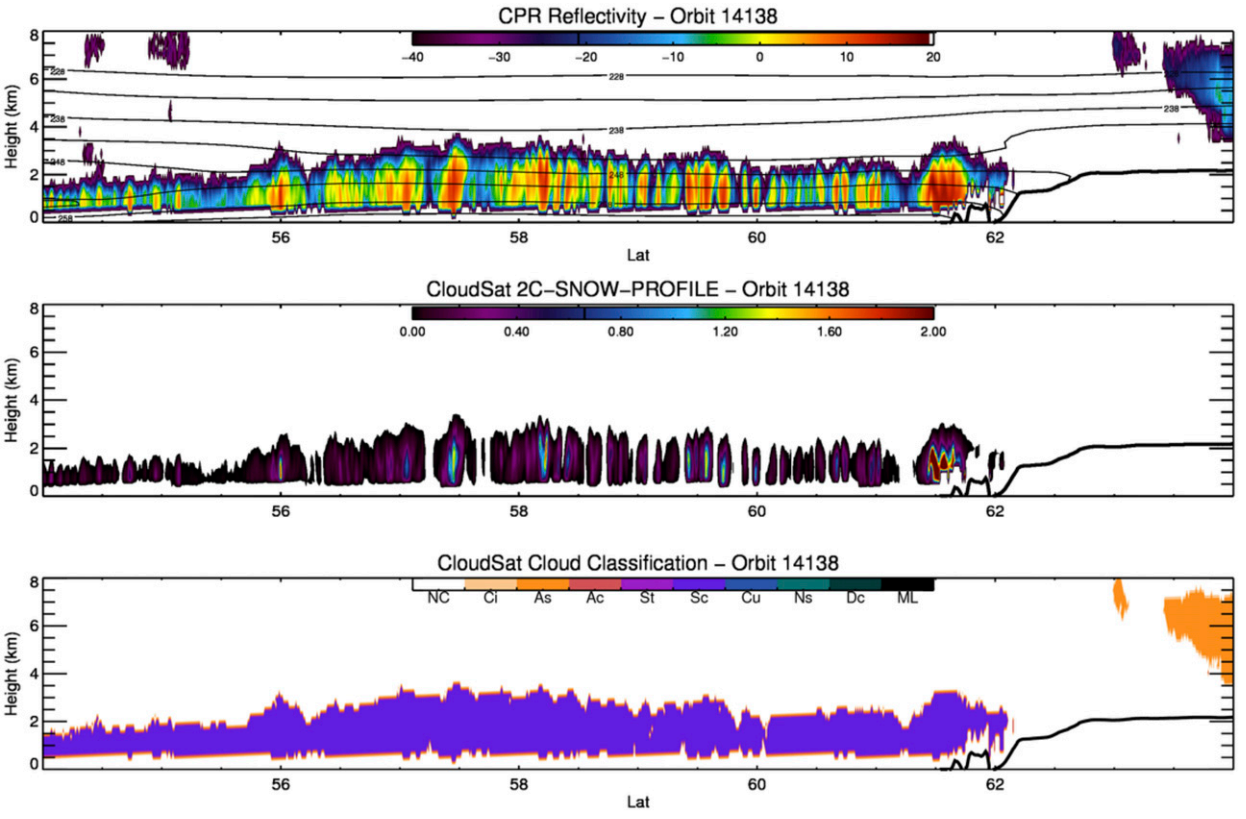

FIG. 2. (top) *CloudSat* CPR reflectivity factor (dBZ) profiles from the 2B-GEOPROF product, (middle) snowfall rate retrievals (mm h^{-1}) from the 2C-SNOW-PROFILE product, and (bottom) cloud classifications from the 2B-CLDCLASS product for a section of orbit 14138 on 24 Dec 2008. ECMWF temperature profiles (K) are also shown in the top (thin black lines). The thick black solid line is Greenland's land surface from the digital elevation database contained in the 2B-GEOPROF product. Abbreviations for the different cloud classification categories are provided in Table 2. This case is predominantly classified as stratocumulus (Sc).

heights lower than 5 km. Furthermore, shallow snow occurrences were further subdivided into isolated (<40 km) versus extended (>40 km) categories based on the horizontal radar reflectivity continuity. The Wang et al. (2013) analysis focused on cloud liquid water content trends in the shallow versus deep cloud structures, with direct applications to passive microwave remote sensing. Note that the Wang et al. (2013) snowfall event partitioning methodology would most likely produce a different spatial shallow snowfall occurrence map when compared to the results presented in section 3. For instance, any nimbostratus snowfall events with cloud-top heights lower than 5 km would be classified as shallow events using the Wang et al. (2013) methodology. The shallow cumuliform versus nimbostratus categories are preferred for this study since we are most interested in discriminating shallow convective cumuliform clouds from nonconvective snowfall.

Figures 2–4 show three snowfall cases near Greenland to highlight typical structures associated with shallow cumuliform and nimbostratus snowfall events, thus providing valuable context to the global snowfall partitioning results presented in section 3. Figure 2 (from *CloudSat* orbit 14138 on 24 December 2008) is an illustrative shallow cumuliform snowfall case. Figure 2 shows convective snow forced by a postfrontal cold-air outbreak interacting with unfrozen North Atlantic Ocean waters near Greenland (the Greenland coastline and land surfaces are indicated by the thick black line at the northernmost latitudes). Cloud-top heights for this event are confined to less than ~2–3 km AGL, and the cellular convective nature of this snowfall event is an obvious defining feature. Maximum CPR radar reflectivities exceed ~15 dBZ in the convective cores, with corresponding 2C-SNOW-PROFILE liquid equivalent snowfall rate retrievals between 1 and 2 mm h^{-1}. The 2B-CLDCLASS product labels these shallow convective clouds as stratocumulus structures, and the snowfall partitioning scheme thus places them in the shallow cumuliform snowfall category.

Figure 3 is a continuation of the same orbit shown in Fig. 2 (note the 64°N latitude end and start point for each

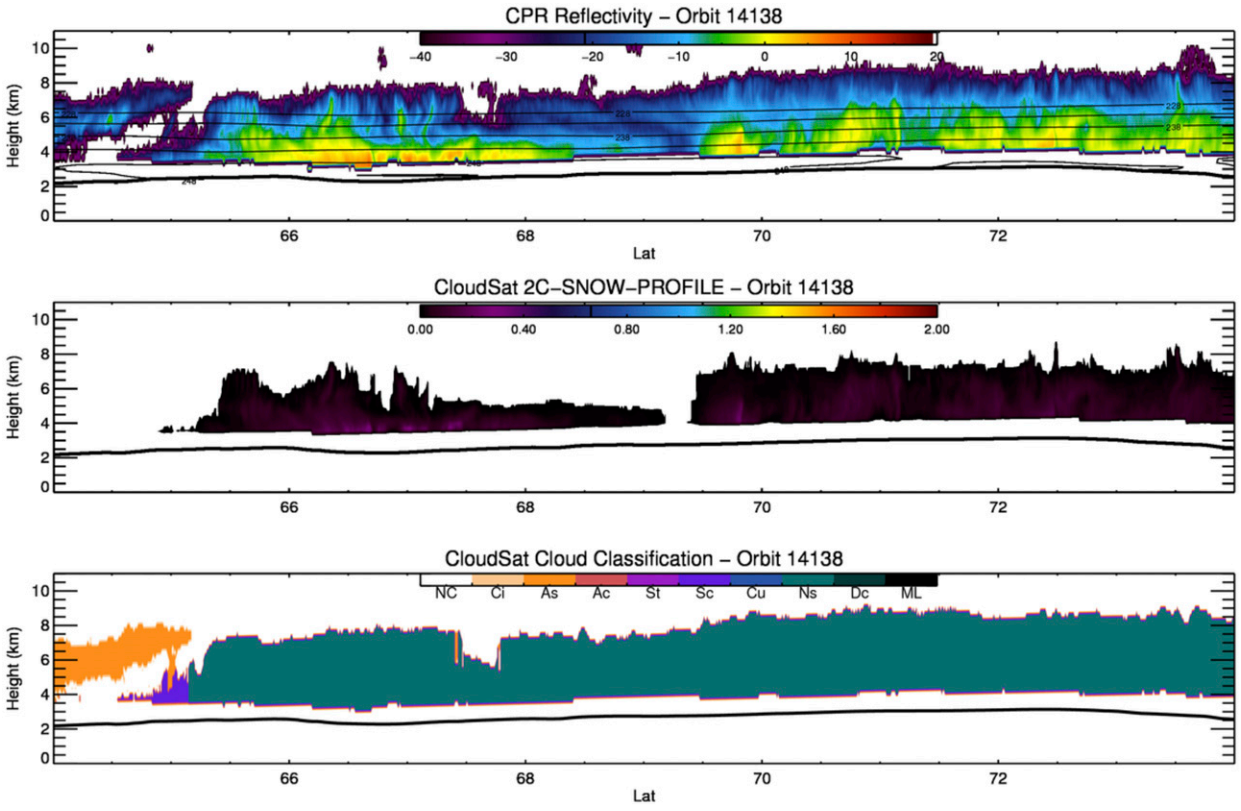

FIG. 3. As in Fig. 2, but for a synoptic snowfall event over Greenland. This is a continuation of the same orbit shown in Fig. 2 as *CloudSat* traverses Greenland. This case is predominantly classified as nimbostratus (Ns) cloud structures.

respective figure), but this section of the *CloudSat* overpass is entirely over the Greenland Ice Sheet and captures a large-scale snowfall event associated with a midlatitude cyclone. Cloud-top heights are generally between 4 and 6 km AGL over the ice sheet. Fall streaks emanating from small-scale upper atmosphere convective cells are apparent throughout much of this segment of the snowfall event, similar in appearance to the snowfall-generation processes associated with the cold sector of a midlatitude winter cyclone described by Rauber et al. (2014). Maximum near-surface reflectivities are generally below ~10 dBZ, with a few embedded regions exceeding 10 dBZ. *CloudSat*-derived snowfall rates are fairly light and do not exceed ~0.4 mm h^{-1} for the entire span shown. Because of the extended cloud-top heights and mostly contiguous radar reflectivity field, the 2B-CLDCLASS product indicates mostly nimbostratus cloud structures for the vast majority of the precipitating observations shown in Fig. 3. The only nimbostratus exception affiliated with this snowfall event is located at the far southernmost edge of the cloud structure that is labeled as stratocumulus where cloud-top heights are much lower.

Figure 4 shows a final *CloudSat* overpass on 24 December 2008 (orbit 14144) that again captures ocean-induced convective snowfall near Greenland. Similar to Fig. 2, the convective cores contain elevated reflectivities (exceeding ~15 dBZ) and retrieved snowfall rates (>2.0 mm h^{-1}). The convective snow shown in Fig. 4 is more vigorous than the earlier *CloudSat* overpass, as cloud-top heights approach ~4 km. The 2B-CLDCLASS product, however, indicates a mixture of cumulus and stratocumulus cloud structures associated with this overpass segment due to subtle differences in reflectivity composition or cloud-top height/temperature. Such differences in cloud classifiers are irrelevant for the purposes of this study, however, since both cumulus and stratocumulus classes are considered shallow cumuliform clouds in the snowfall partitioning criteria. The cloud structures shown in Fig. 4 possess similar cloud forcing mechanisms due to air–sea interactions and are most likely microphysically similar mixed-phase clouds.

c. Geographical gridding methodology

CloudSat's CPR is a nonscanning, near-nadir-pointing radar with a 16-day orbital cycle. Figure 5 shows 2006–10 *CloudSat* orbital tracks to illustrate the coverage provided by the 16-day orbital cycle over two different regions (Greenland–Iceland–North Atlantic Ocean and

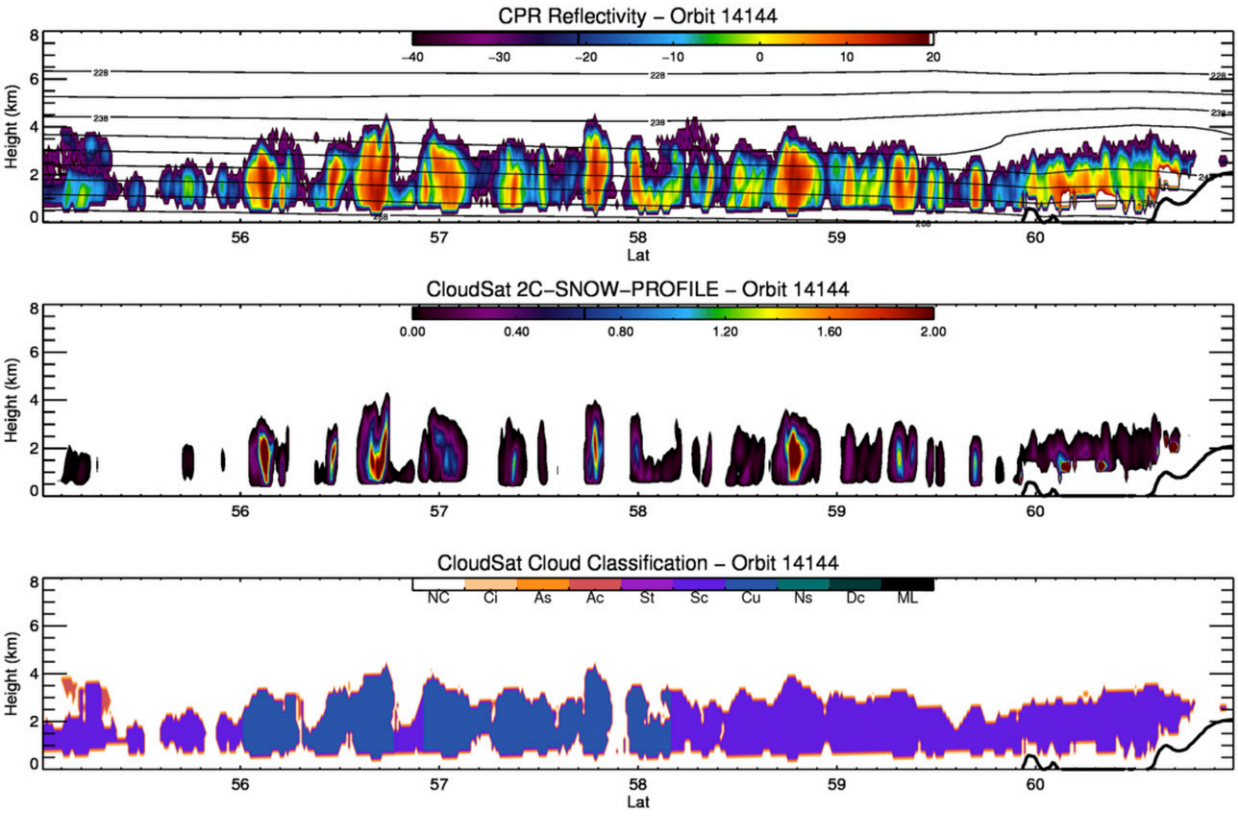

FIG. 4. As in Fig. 2, but for orbit 14144 on 24 Dec 2008. The coast of Greenland is shown on the far right. This case is classified as a mixture of stratocumulus and cumulus cloud structures.

western Pacific Ocean). *CloudSat* observations are gridded into 1° × 1° boxes for many of the results presented in section 3. *CloudSat*'s coverage is limited to latitudes from 82°N to 82°S, so any gridded products will not contain data exceeding these latitudinal limits. High-latitude areas systematically receive more *CloudSat* overpasses and denser spatial coverage compared to equatorward latitudes. As shown in Fig. 5, intersecting *CloudSat* orbital tracks create local maxima that inflate the population of data points in a given 1° grid box. These nodal points are obvious features at equatorward latitudes. High-latitude grid boxes contain over 20 000 observations at maximal poleward locations (near 82° latitude) for the 2006–10 period, while midlatitude grid boxes contain a wide sampling range between ~5000 and over 15 000 observations per grid box depending on the proximity to overlapping orbital track nodes.

3. Results

a. Global snowfall analysis

A multiyear perspective of all snowfall events contained in the *CloudSat* snowfall database is first presented in this section. Similar to the shorter-duration snowfall datasets analyzed in earlier *CloudSat* snowfall studies (e.g., Liu 2008; Hiley et al. 2011), the number of *CloudSat*-indicated snowfall events generally increases poleward in each hemisphere (not shown). The highest counts (>10 000 snowfall events per grid box) occur near 82° latitude in the Northern Hemisphere because of both the higher likelihood of snowfall and increased *CloudSat* sampling at poleward latitudes (not shown). Localized snowfall count maxima exceeding 5000 counts also occur in some other regions away from higher latitudes (e.g., Southern Hemispheric oceans, North Atlantic Ocean, western Pacific Ocean, Canadian–Alaskan Pacific coastline, southern Greenland, and continental Asia). *CloudSat* sampling gaps equatorward of ~50° in both hemispheres also exist. Larger grid boxes would mitigate these sampling artifacts, but 1° grid sizes are deemed useful to analyze higher-latitude snowfall with greater spatial resolution.

CloudSat-derived snowfall fractions are shown in Fig. 6a, where snowfall fraction is defined as the ratio of snowfall events to the total number of *CloudSat* observations in each grid box. Snowfall fraction values are the

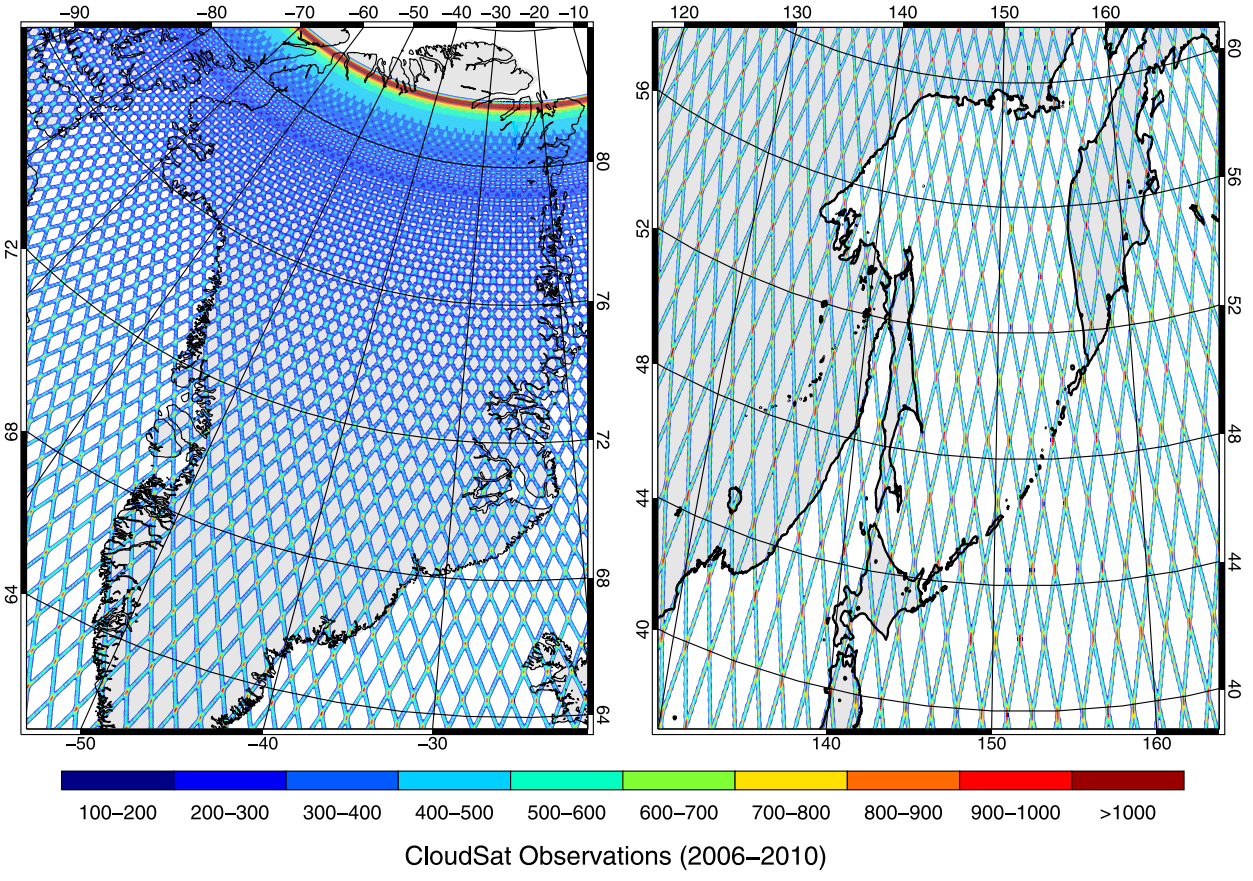

FIG. 5. The total number of *CloudSat* observations in the (left) North Atlantic Ocean near Greenland and Iceland and (right) western Pacific Ocean for the 2006–10 period used in this study. *CloudSat* orbital swaths associated with its 16-day orbital cycle are indicated, with observational maxima occurring at orbital crossover nodes.

preferred method to interpret the *CloudSat* snowfall dataset since latitudinal sampling differences are minimized. Unlike total snowfall counts, the maximum snowfall fraction values are not exclusively anchored to poleward latitudes near 82°. Notable snowfall fraction maxima exceeding 30% are found in the transoceanic Southern Hemisphere storm-track region between ~60° and 70°S latitudes. Past studies have indicated similar inflated snowfall fraction magnitudes in this region using the first year or two of *CloudSat* observations (Liu 2008; Ellis et al. 2009; Hiley et al. 2011). Notably, a pronounced snowfall fraction decrease in the Southern Hemispheric latitudinal belt is located in the vicinity of the Ross Sea (75°S, 175°W) and on the lee side of the Antarctic Peninsula (70°S, 65°W) over the Weddell Sea (75°S, 45°W). While the largest Southern Hemispheric snowfall fractions are located over the oceans, continental snowfall maxima over Antarctica are located near the Antarctic Peninsula and Amundsen Sea (73°S, 110°W) coastal regions. A large snowfall fraction gradient also exists between the coast and interior regions of Antarctica, similar to findings presented in Palerme et al. (2014) and Milani et al. (2015).

Northern Hemispheric snowfall fraction values are lower, on average, compared to the Southern Hemisphere. Notable over-ocean snowfall fraction maxima exceeding 30% are located in the North Atlantic Ocean over the Greenland (75°N, 8°W) and Barents (75°N, 40°E) Seas, while overland snowfall fraction maxima of similar magnitudes are found in a thin strip along the Alaskan and Canadian Pacific coastline and various Greenland regions, especially the southeastern Greenland coastal region. A large swath of the high-latitude Northern Hemisphere contains snowfall fractions near or exceeding 20%, though, including vast regions of the Arctic Ocean, the western Pacific Ocean near Kamchatka (57°N, 160°E), interior Russia (65°N, 90°E), the Himalayan Mountains and nearby Tibetan Plateau, the Norwegian coast (60°N, 8°E), interior northern Canada (Yukon and Northwest Territory regions; 65°N, 135°W), and coastal and interior eastern Canada (Newfoundland, Labrador, and Quebec; 55°N, 65°W).

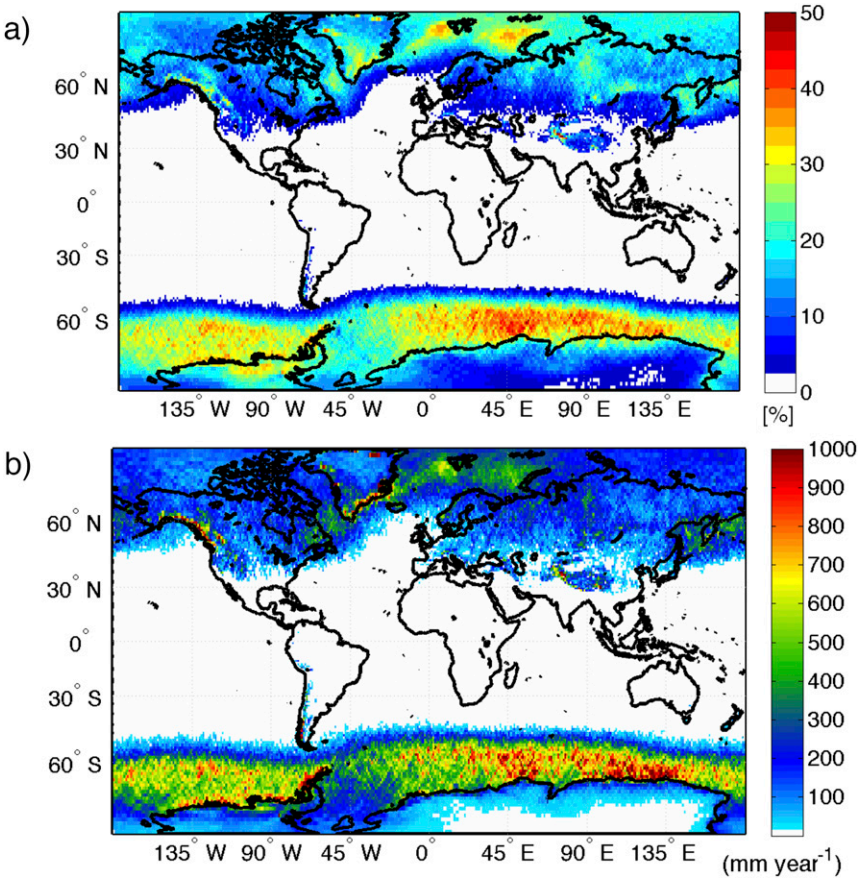

FIG. 6. *CloudSat*-derived (a) snowfall fraction (%) and (b) mean annual liquid equivalent snowfall (mm yr^{-1}) in 1° × 1° bins for the 2006–10 dataset. Snowfall fraction is defined as the number of snowfall events divided by the total number of observations in each grid box.

Complementing the snowfall fraction analysis presented in Fig. 6a, mean annual snowfall rates (liquid equivalent) derived from 2C-SNOW-PROFILE retrievals are shown in Fig. 6b. The highest estimated 2006–10 mean annual snowfall rates (>1000 mm yr^{-1}) coincide with many of the regions previously highlighted. These snowfall rate estimates are associated with considerable uncertainties exceeding 50% [see Palerme et al. (2014) for sample *CloudSat* snowfall estimate uncertainties and Kulie and Bennartz (2009), Hiley et al. (2011), and Wood et al. (2013) for further discussion of *CloudSat* snowfall retrieval uncertainties due to underlying microphysical assumptions]. The Southern Hemispheric snowfall belt is again a defining feature of this near-global map. The latitudinal belt between ~60° and 70°S receives the largest amount of snowfall, and the oceanic versus continental gradient near and over Antarctica—as well as the Ross and Weddell Sea snowfall minima—are defining features of Southern Hemispheric snowfall distribution. An enhanced Northern Hemispheric snowfall belt occurs from the eastern Canadian provinces northeastward to the extreme North Atlantic Ocean and Barents Sea. The southeast Greenland and Alaskan/Canadian coasts also receive substantially elevated snowfall totals, while the western Pacific Ocean near Kamchatka experiences mean annual snowfall totals exceeding 400 mm yr^{-1}. Central Russia and the Himalayan region, both interior continental locations, receive over 400 and 600 mm yr^{-1} of estimated snowfall, as do isolated mountainous regions in both hemispheres. Vast areas of continental North America, Europe, and Asia average between 50 and 300 mm yr^{-1} of snowfall. The Arctic Sea region north of Russia has a relatively homogenous estimated average annual snowfall rate between 150 and 300 mm yr^{-1}, while the Arctic Sea north of Alaska and Canada generally receives less snowfall (<150 mm yr^{-1}).

b. *Snowfall partitioning: General statistics*

Table 2 contains frequency of occurrence statistics for 2B-CLDCLASS categories associated with orbital (ungridded) *CloudSat*-detected snowfall events. The entire

TABLE 2. Number (N) and percentage of *CloudSat*-observed snowfall events associated with various 2B-CLDCLASS cloud categories.

2B-CLDCLASS category	N	Percentage of *CloudSat*-observed snowfall events
Stratocumulus (Sc)	1.706×10^7	34.22%
Cumulus (Cu)	7.080×10^5	1.42%
Total shallow cumuliform	1.777×10^7	35.64%
Total nimbostratus (Ns)	2.948×10^7	59.13%
Altostratus (As)	8.775×10^5	1.76%
Altocumulus (Ac)	6.631×10^5	1.33%
Deep cumulus (Dc)	8.476×10^4	0.17%
No classification (NC)	9.822×10^5	1.97%
Total other	2.608×10^6	5.23%
Total	4.986×10^7	100%

CloudSat snowfall dataset for the 2006–10 period contains over 49 million probable snowfall events. Shallow cumuliform snowfall comprises ~36% of the *CloudSat* snowfall dataset, while nimbostratus snowfall events occur more frequently (~59%). The vast majority of shallow snowfall cases are labeled as stratocumulus (~34% of overall database), with a much smaller fraction identified as cumulus (~1.4%) cloud structures.

The shallow cumuliform and nimbostratus snowfall categories comprise over 95% of the *CloudSat* snowfall dataset, but did not account for all snowfall events in the database. Interestingly, a few other 2B-CLDCLASS categories populate the snowfall database, including altostratus (1.8%), altocumulus (1.3%), and clear/no classification (~2%). The true definition of altostratus and altocumulus clouds as elevated cloud structures should preclude their association with surface precipitation. The 2B-CLDCLASS product, however, designates some near-surface clouds associated with possible surface snowfall events as alto-type clouds. Altostratus and altocumulus snowfall events occur around the globe in mostly small numbers, but higher occurrences of these snowfall categories appear over extremely cold surfaces like interior Antarctica and Greenland, as well as the pan-Artic region near 82°N (not shown). The 2B-CLDCLASS alto-type snow categories are most likely due to snow-producing clouds in very cold ambient environments, often located at high elevations. These categories are not included in the global spatial maps presented in following sections, although the altostratus cases could arguably be associated with the nimbostratus category since, after inspecting numerous *CloudSat* overpasses of such events, they seem structurally similar to typical nimbostratus snowfall-producing clouds (not shown). Although snowfall rates associated with alto-type and no cloud classification categories are generally very light, further partitioning studies over Greenland or Antarctica should include these categories to fully account for all snowfall events in these regions. All other 2B-CLDCLASS categories (deep cumulus, stratus, cirrus, and mixed layer) have negligible occurrence rates. These cloud categories will not be considered in the following analyses.

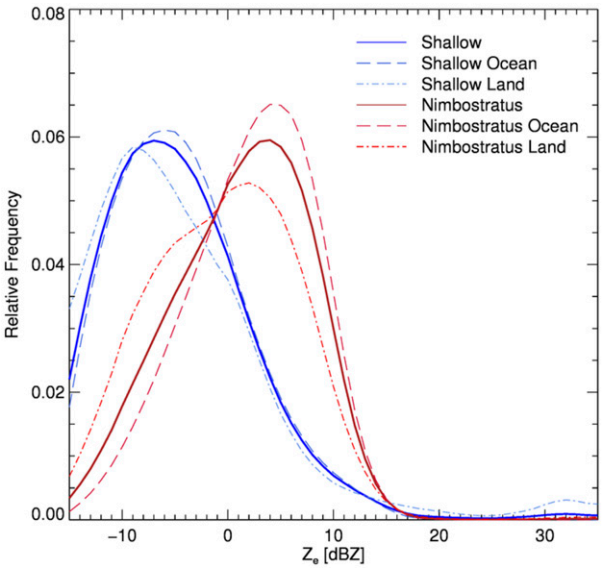

FIG. 7. *CloudSat* CPR near-surface reflectivity factor distributions for all shallow cumuliform (thick blue) and nimbostratus (thick red) snowfall cases. Additional distributions for shallow cumuliform snowfall events over ocean (blue dashed) and land (blue dash–dotted), as well as nimbostratus snowfall events over ocean (red dashed) and land (red dash–dotted), are also shown. A radar reflectivity bin size of 1 dBZ is used to create the respective distributions. The reflectivity distribution is truncated at −15 dBZ since *CloudSat* precipitation products use this value as a minimum threshold to be considered a likely precipitation observation.

Figure 7 highlights near-surface CPR reflectivity distributions partitioned by snowfall mode and indicates systematic trends in snowfall intensity associated with shallow cumuliform versus nimbostratus snowfall events. The nimbostratus snowfall category is associated with much higher radar reflectivities and associated snowfall rates, with a reflectivity distribution peak near 4 dBZ. While Figs. 2 and 4 show intense shallow snowfall events, the entire population of global shallow cumuliform snowfall events displays lighter reflectivities than the nimbostratus snowfall category and is associated with a reflectivity peak from near −7 to −8 dB. To further illustrate the frequency of very light, shallow snowfall events globally, about 74% (96%) of shallow snow-related CPR observations are below the 0 (10) dBZ threshold, while 37% (91%) of nimbostratus snowfall events do not exceed the same reflectivity thresholds.

Figure 7 indicates systematic intensity differences between the two snowfall modes. Interesting fractional reflectivity trends, however, are associated with elevated reflectivities. While over-ocean/water shallow cumuliform snowfall events are associated with larger peak reflectivity values compared to land, this trend reverses for radar reflectivities exceeding about 14 dBZ. Additionally, the shallow cumuliform snowfall category exhibits an increased reflectivity fraction above about 17 dBZ over land surfaces (blue dash–dotted line in Fig. 7) compared to the nimbostratus category. A secondary overland shallow snowfall radar reflectivity peak also exists at values exceeding 30 dBZ. This secondary peak is an obvious ground clutter signature, as W-band snowfall-related reflectivities cannot theoretically exceed ~20 dBZ because of non-Rayleigh scattering effects (e.g., Matrosov 2007; Kulie and Bennartz 2009). A very small percentage of the *CloudSat* snowfall database therefore requires further clutter mitigation. Ground clutter associated with abrupt topographical changes may also elevate overland shallow reflectivities under 20 dBZ, but the overland reflectivity increase between about 14 and 20 dBZ may also be plausibly explained by land/orographic enhancement. Further research beyond the scope of the current study is needed to determine the exact cause of the overland shallow snowfall reflectivity behavior.

Irrespective of overland shallow snowfall, overwater shallow snowfall contains a slightly higher fraction of reflectivities exceeding about 15 dBZ compared to the nimbostratus category. This feature most likely reflects intense lake- or ocean-effect snow events as indicated in Figs. 2 and 4. Liu (2008) also found a similar shallow snowfall signature in the highest snowfall rates derived from *CloudSat* observations. Similar to shallow snowfall, deeper nimbostratus snowfall structures exhibit a slight land (~3 dBZ) versus ocean (~5 dBZ) reflectivity distribution peak difference. The overland nimbostratus snowfall category also displays a subtle secondary "shoulder" near −6 dBZ associated with lighter nimbostratus snowfall that commonly occurs over cold continental regions like interior Antarctica and eastern Russia (not shown). The shallow snowfall category is dominated by ocean/water events (~71%) compared to overland events (~29%) from a frequency of occurrence perspective. The nimbostratus snowfall dataset has a reduced ocean (~62%)–land (~38%) occurrence discrepancy compared to shallow cumuliform snowfall.

c. *Snowfall partitioning: Global analysis*

Figure 6 from the previous section shows the global snowfall viewpoint from *CloudSat* spaceborne measurements. This study, however, also assesses whether *CloudSat* can effectively discriminate between different snowfall modes to provide a global shallow snowfall census. Based on previous observational studies, a strong shallow cumuliform snowfall signal should exist over large bodies of water at higher latitudes because of lake- or ocean-forced convective snow (e.g., Figs. 2, 4). Previous observational studies have not, however, determined shallow snowfall frequency or estimated its contribution to total annual snowfall accumulation on a global basis.

Using the snowfall partitioning methodology outlined in section 2, Figs. 8 and 9 present direct evidence that shallow cumuliform snowfall plays a prominent role in global surface snowfall production. Figure 8 illustrates the fraction of snowfall events that are associated with shallow cumuliform and nimbostratus clouds, respectively, for the entire *CloudSat* snowfall database. The most striking feature shown in Fig. 8 is the stark oceanic versus continental difference between shallow and nimbostratus snowfall fraction, with the open ocean serving as the obvious forcing mechanism to inflate shallow snowfall fraction in many regions. Similarly, Fig. 9 clearly shows the oceanic versus continental dichotomy between mean annual estimated snowfall rate due to nimbostratus and shallow events. Deeper nimbostratus snowfall dominates the contribution to annual snowfall totals presented in Fig. 9b over most continental regions and regions frequently covered by sea ice, while shallow snowfall contributes significantly to annual snowfall totals in select over-ocean regions. While shallow snowfall frequently occurs in many global locations (Fig. 8a), it comprises ~18% of the estimated annual global surface snowfall input for the 2006–10 *CloudSat* dataset, compared to ~82% for nimbostratus snowfall. These global percentages discount snowfall events associated with other 2B-CLDCLASS categories, which at most comprise another ~1%–2% of annual global snowfall contribution.

In the Northern Hemisphere, large landmasses are typically dominated by nimbostratus snowfall events from both frequency (Fig. 8b) and estimated annual snowfall rate (Fig. 9b) perspective. Distinct land–ocean gradients between shallow and deep snowfall zones also exist in numerous locations. Prominent Northern Hemispheric regions that experience both frequent snowfall (Figs. 6a,b) and widespread shallow snowfall fraction values exceeding 60% include:

- a southwest-to-northeast-oriented swath from the North Atlantic Ocean to Barents Sea from about 45°W to 70°E longitude;
- the Labrador Sea between Greenland and Canada (60°N, 55°W);
- the western Pacific Ocean, including the Seas of Okhotsk (55°N, 150°E) and Japan (40°N, 135°E); and
- the southern Bering Sea between Siberia and Alaska (58°N, 180°).

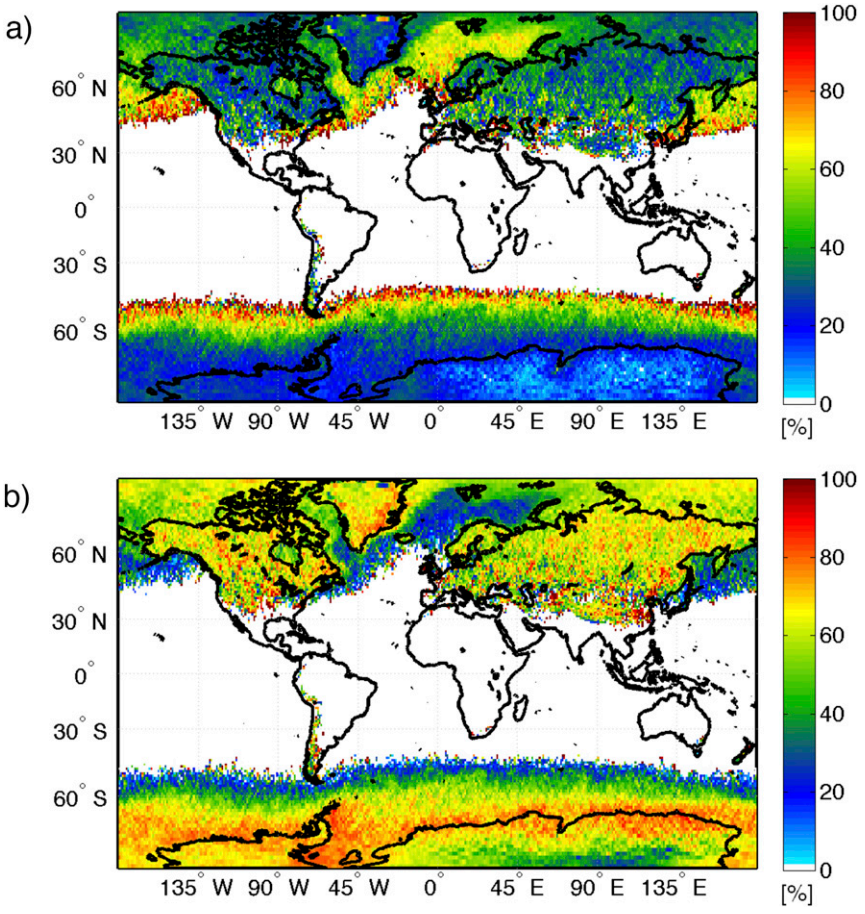

FIG. 8. *CloudSat*-observed (a) shallow cumuliform snowfall fraction and (b) nimbostratus snowfall fraction for the entire 2006–10 dataset. Shallow cumuliform and nimbostratus snowfall categories are defined by cloud classifications from the 2B-CLDCLASS product. See text for further details.

These Northern Hemispheric regions consistently receive ~40%–60% of estimated annual snowfall accumulation from shallow snowfall (Fig. 9a). The Great Lakes region also contains many grid boxes with shallow snowfall fractions exceeding 60%, but its comparatively small geographical footprint makes it difficult to discern on global maps. The Great Lakes region has motivated significant shallow cumuliform snowfall research (see references in the introduction), but this region pales in comparison to high-latitude over-ocean regions that experience significant amounts of shallow cumuliform snow over vast geographical expanses.

A common trait shared among the peak oceanic shallow snowfall regions is reduced or negligible winter sea ice coverage. Other oceanic Northern Hemispheric areas are associated with somewhat elevated shallow snow fractions exceeding ~40% [e.g., Hudson Bay (60°N, 85°W), Baffin Bay (73°N, 67°W), the Arctic Ocean near Alaska and eastern Siberia, and Kara Sea (77°N, 77°E)], but increased ice cover most likely diminishes shallow snowfall production compared to the peak regions previously mentioned. This potential shallow snowfall–sea ice relationship will be discussed further in section 4. Many Northern Hemispheric continental regions also display shallow cumuliform snowfall fractions exceeding 40%, especially many locations over Russia, Europe, north-central Greenland, and mountainous regions of North America (Fig. 8). The contribution to annual snowfall from shallow events is typically depressed in these regions, thus indicating light snowfall rates associated with shallow cumuliform snow (Fig. 9).

Unlike the complicated and regionally variable Northern Hemispheric shallow snowfall pattern, the Southern Hemisphere displays a fairly uniform shallow snowfall frequency (Fig. 8) and contribution to annual snowfall (Fig. 9) gradient from north to south, with equatorward latitudes receiving more shallow snowfall events and surface precipitation flux from shallow snow. The high

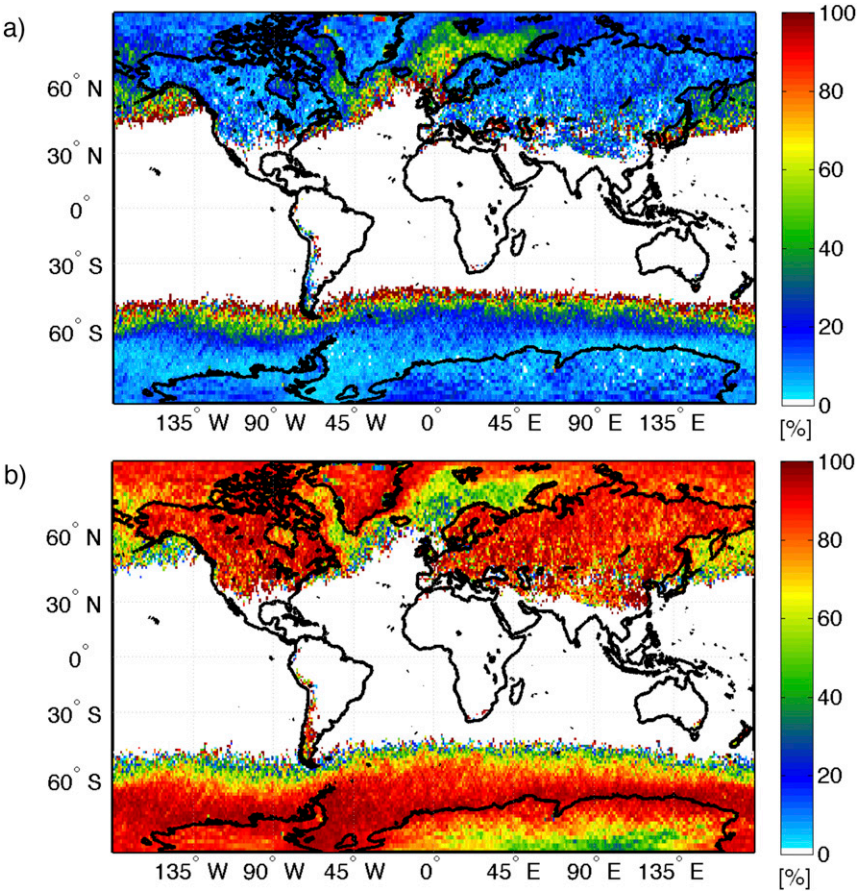

FIG. 9. Percentage of annual estimated snowfall accumulation attributed to (a) shallow cumuliform and (b) nimbostratus snowfall events.

snow fraction 60°–70°S storm-track region highlighted in Fig. 6 receives most of its annual estimated snowfall accumulation from deeper snowfall events. A few areas near and over Antarctica display slightly higher shallow snowfall fractions (e.g., Antarctic Peninsula, Ross Sea region, and near-coastal regions at ~20°W longitude) and slightly reduced contributions to annual snowfall from deeper snowfall, but deep snowfall consistently contributes greater than 60% to the total annual snowfall in most Antarctic regions.

Figures 8 and 9 also show thin swaths located at equatorward latitudes in both hemispheres that experience shallow snowfall almost exclusively. These fringe regions, however, receive relatively few *CloudSat*-indicated snowfall events. When it snows in these locations, it is most likely to be from shallow cumuliform clouds, but annual accumulations are usually minimal (Fig. 6b).

d. Snowfall partitioning: Greenland focus

Figures 6–9 illustrate the multiyear *CloudSat* snowfall dataset from a global perspective, but it is also useful to focus regionally to elucidate details that are difficult to distinguish from the global figures. Figure 10 shows shallow cumuliform and nimbostratus snowfall fraction and mean annual snowfall rate percentage, respectively, near and over Greenland. This region was highlighted in Figs. 6–9 for receiving frequent and abundant snowfall from both shallow (ocean) and deeper nimbostratus (over land and Greenland ice sheet) snowfall. Accumulating snowfall also plays an important role in the Greenland ice sheet mass balance (e.g., Shepherd et al. 2012; Castellani et al. 2015), and snowflake production effectively scavenges supercooled liquid water in high-latitude mixed-phase clouds (e.g., Shupe et al. 2006), thus making this region interesting from multiple scientific perspectives.

Figure 10 highlights a few key features over and surrounding Greenland that warrant further discussion. For instance, the shallow snowfall signature fraction and annual accumulation percentage maxima in the Labrador Sea southwest of Greenland contains snowfall fractions exceeding 70% (Fig. 10a) and estimated accumulation percentages greater than 60% (Fig. 10c). There is also a latitudinal dividing line at ~65°N where shallow snowfall

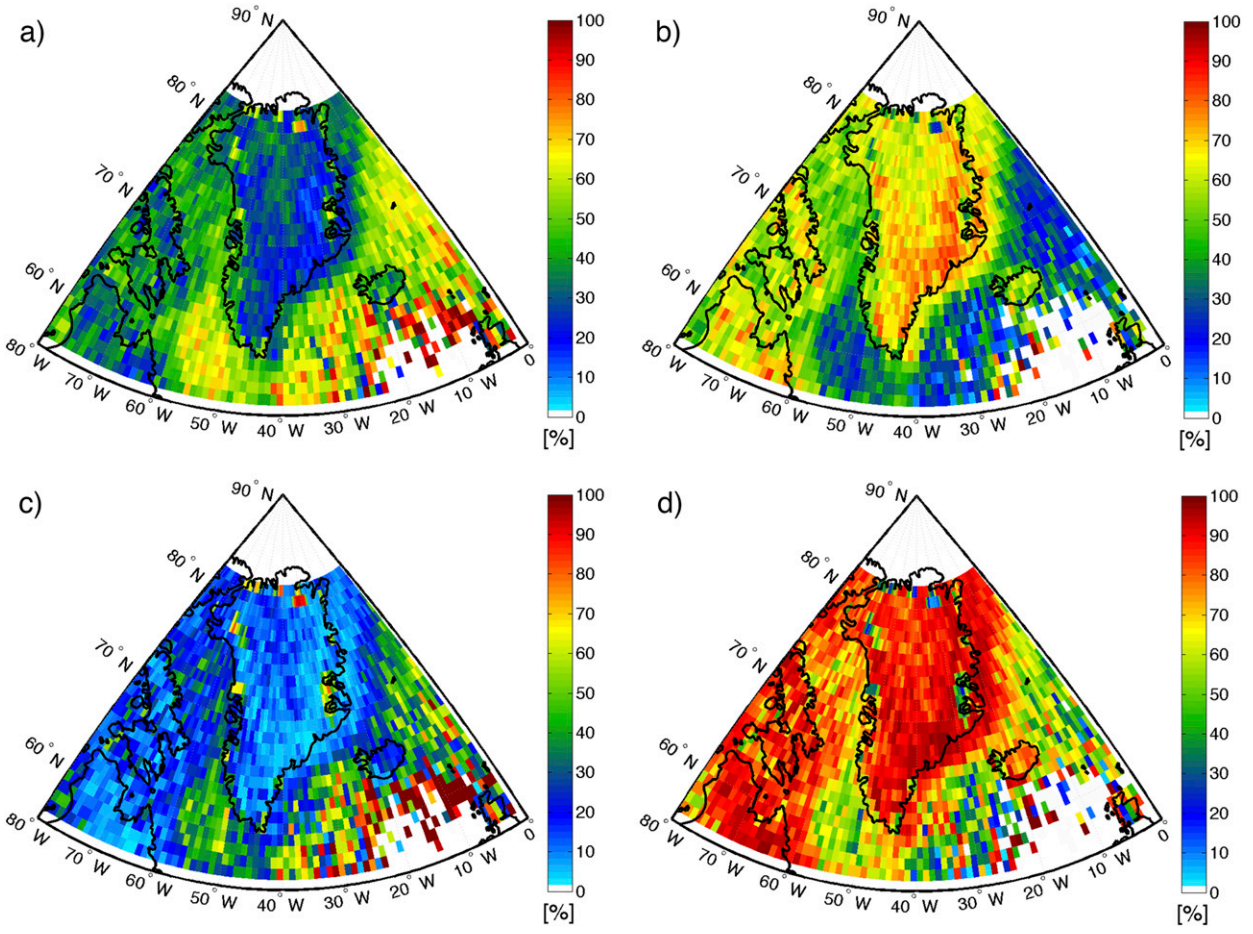

FIG. 10. (a) Shallow cumuliform snowfall fraction, (b) nimbostratus snowfall fraction, and percentage of annual snowfall attributed to (c) shallow cumuliform and (d) nimbostratus snowfall events near and over Greenland.

frequency (accumulation percentage) decreases to mostly under 40% (30%), with a few isolated pixels indicating slightly higher values. This transition from very high to slightly lower shallow snowfall fractions is aligned with the typical maximal sea ice extent between Baffin Bay and the Labrador Sea (see, e.g., National Snow and Ice Data Center monthly ice coverage maps for further details; https://nsidc.org/data/seaice_index/).

The sharp oceanic versus continental shallow snowfall fraction gradient evident near Greenland in Fig. 8 was previously discussed, but details of this gradient over Greenland are difficult to discern in the global map. Since *CloudSat* products utilize a higher vertical bin over land versus ocean to retrieve snowfall rates, a natural question to pose is whether this land–ocean gradient is amplified by utilizing different vertical bins over different surfaces (i.e., are there less shallow snowfall events over land because of a more restrictive vertical data bin policy applied to land vs ocean observations?). Figure 10, however indicates a relatively thin inland zone of increased shallow snowfall fractions over the west Greenland coast, especially in the northernmost coastal regions near 77°–78°N and Greenland coastal latitudes south of ~70°N. The inland shallow snowfall fraction values are similar to nearby overwater fraction magnitudes and do not indicate land versus water shallow snowfall detection artifacts in this region. Note, however, that this feature is less prominent in the annual accumulation percentage fields. Similarly, Greenland's eastern coast and near-coastal oceanic regions are associated with an obvious shallow cumuliform snowfall shadow, where nimbostratus snowfall structures are prominent compared to shallow cumuliform snow (Figs. 10b,d). This signature is interpreted as a region where convective snow does not readily form close to shore because of increased seasonal ice coverage and/or the lack of significant overwater fetch needed for convective snow showers to form when cold air advects over ice-free water.

A few other inland Greenland snowfall features are also evident in Fig. 10. First, an apparent orographic

snowfall signature is located in southeast and central-east Greenland regions where a gradient in the nimbostratus snow category exists (Figs. 10b,d). This region is one of the snowiest locations in the Northern Hemisphere, similar to other observational and modeling studies over Greenland (Hanna et al. 2006), and is dominated by homogenous and deeper snowfall structures. Second, a large swath of interior north-central Greenland is associated with 30%–40% cumuliform snowfall fractions. This shallow snowfall influence, however, is not reflected as obviously in the accumulation partitioning statistics, as the nimbostratus snow category contributes a disproportionate percentage to the estimated annual snowfall in this region. *CloudSat* appears to capture lightly precipitating, shallow events over the Greenland ice sheet that might be associated with shallow mixed-phase Arctic clouds (e.g., Shupe et al. 2006, 2013). Further investigation is necessary to confirm this finding, including detailed analyses of *CloudSat* overpasses in this region. Finally, some Greenland locations are still affected by ground clutter contamination even after adopting a more rigorous approach to detect and mitigate ground clutter compared to previous *CloudSat* snowfall studies. Figure 10 indicates a few isolated near-coast Greenland pixels where shallow snowfall fraction is extremely inflated, but these points are located within a broader nimbostratus-dominated region. Further clutter mitigation steps should be developed to completely remove these data points from the *CloudSat* snowfall dataset.

4. Conclusions

The *CloudSat* observational dataset provides the first opportunity to study near-global snowfall, and numerous recent investigations have utilized *CloudSat* for snowfall-related research. This study leverages *CloudSat* cloud classification and snowfall rate retrieval products to partition 2006–10 *CloudSat* snowfall observations into shallow cumuliform and nimbostratus snowfall categories, thus creating a unique global census of shallow cumuliform snowfall events. Cumuliform, snow-producing cloud structures display a narrow cloud thickness distribution centered near 1.5 km, while nimbostratus snow-producing clouds exhibit a much broader cloud thickness distribution that peaks near 4 km, thus confirming the notion of two disparate snow-producing cloud types separated both by cloud macrophysical (e.g., cloud thickness plus 2B-CLDCLASS descriptors) and mechanistic (e.g., cloud forcing) properties. Shallow snowfall associated with cloud structures identified as stratocumulus and cumulus (nimbostratus) clouds are shown to globally comprise ~36% (~59%) of the 2006–10 *CloudSat* snowfall dataset by occurrence, while constituting ~18% (82%) of the estimated annual global snowfall accumulation in liquid equivalent terms. Certain high snowfall frequency regions, however, experience shallow snowfall occurrence fractions exceeding 60% (e.g., North Atlantic Ocean near Greenland, Barents Sea, western Pacific Ocean, southern Bering Sea, and Southern Hemispheric oceanic storm-track region). These same regions receive an estimated 40%–60% of the annual snowfall accumulation from shallow cumuliform cloud structures. Many other regions also display localized increases in shallow snowfall frequency and accumulation percentage. About 71% (29%) of shallow snowfall events occur over water (land) surfaces, and distinct land–water gradients exist in global shallow snowfall fraction and accumulation percentage maps.

CloudSat Cloud Profiling Radar reflectivity distributions also reveal that shallow snowfall is much lighter, on average, than deeper nimbostratus events—with the possible exception of a high-reflectivity shallow snowfall mode associated with CPR reflectivities exceeding ~15 dBZ that might reflect intense inland lake- or ocean-effect snow. This study also reveals that shallow snowfall events are disproportionately associated with light reflectivity values. About 74% (96%) of all shallow cumuliform snowfall events have near-surface reflectivities below 0 (10) dBZ, while ~36% (91%) of nimbostratus snowfall events fall under these same reflectivity levels. These values are extremely useful for the spaceborne radar community to better define future radar capabilities in an effort to remotely sense as much global snowfall as possible. Both shallow and nimbostratus snowfall categories display land versus ocean near-surface reflectivity distribution differences, with oceanic snow associated with mostly higher near-surface CPR reflectivities. The only exception to this trend is a notable increase in near-surface reflectivity fractions above ~14 dBZ for shallow snowfall over land, with a secondary peak at elevated reflectivity values exceeding 30 dBZ. The secondary peak is almost assuredly related to ground clutter, but further investigation is required to understand whether the other overland reflectivity percentage increase is due to land/orographic enhancement to shallow snowfall. Further clutter mitigation techniques can be tested in regions identified by this study to show systematic clutter contamination symptoms.

This study sets the stage for further follow-on methodological, evaluation, and science-related research studies. This dataset can be further parsed to understand the variability and radar/cloud macrophysical properties of shallow snowfall clouds due to environmental parameters (air–sea temperature gradient and stability, low-level humidity, wind speed, etc.). Seasonal variability

of shallow snowfall occurrence and intensity can also be studied, and the potentially intimate relationship between sea ice coverage and shallow snow production can also be isolated. While this study defines cumuliform snowfall as the only ''shallow'' snowfall category, cloud thickness distributions show that over 20% of nimbostratus snow-producing clouds have cloud thicknesses less than 3 km. Further work will be undertaken to understand whether certain areas (mountainous and/or cold, elevated regions like Antarctica) are systematically prone to these types of snowfall events.

The snowfall partitioning statistics presented in this study are derived from *CloudSat* products and their respective inputs, so further work is needed to assess the *CloudSat*-derived results with independent datasets. For instance, future studies will assess whether numerical models realistically represent shallow convective snowfall and global reanalyses datasets (e.g., spatially, seasonally, and from a precipitation intensity and accumulation fraction perspectives). Additionally, ground-based observational datasets are being developed to assess the *CloudSat* partitioning statistics. Long-term, vertically pointing radar datasets are available in some high-latitude regions. These radar observations can readily discriminate snowfall modes and can be exploited as an independent assessment tool (e.g., Kneifel et al. 2011; Castellani et al. 2015). Ground-based operational scanning radar networks can also be used to develop multiyear snowfall partitioning statistics to compare with spaceborne results. Remote sensing datasets with concurrent ground-based snowfall accumulation and microphysical measurements will be especially useful evaluative tools for the *CloudSat*-generated detection and accumulation percentage statistics. It is also conceivable that *CloudSat* understates the occurrence of shallow cumuliform snowfall, as the CPR may not effectively sample extremely shallow snow events because of its overland ''blind zone'' in the lowest ~1 km AGL. Uncertainty analyses will be undertaken using ground-based radars to understand the percentage of extremely shallow snowfall events that may be undetected by *CloudSat* in different meteorological regimes (e.g., Maahn et al. 2014). These independent model and observational datasets will improve snowfall detection uncertainty estimates and identify systematic differences with *CloudSat*-derived partitioned snowfall statistics to isolate the cause of regional or global biases.

This partitioned snowfall dataset also serves as a valuable tool for other applications. For instance, this dataset can also be used for passive microwave snowfall retrieval development and assessment in the GPM era. *CloudSat* and microwave radiometer synergy has already been exploited in the at-launch GPM precipitation retrieval algorithm (Kummerow et al. 2015), as well as in recent studies that document complex radiometric signatures associated with snowfall (Kulie et al. 2010; Liu and Seo 2013). GPM snowfall retrieval algorithm evaluations will be undertaken in regions that are prone to shallow snowfall as identified by this study. Follow-on combined radar–radiometer studies will also be performed to understand whether shallow versus deeper snowfall events exhibit unique multifrequency radiometric signatures that can be exploited to improve microwave radiometer snowfall retrievals.

Acknowledgments. The authors would like to acknowledge the *CloudSat* Data Processing Center for its assistance staging and transferring the various *CloudSat* products used in this study. Constructive comments from three anonymous reviewers are also gratefully acknowledged. This work was partially funded by NASA Grants NNX14AB22G, NNX13AG47G, and NNX12AQ76G.

REFERENCES

Andersson, T., and S. Nilsson, 1990: Topographically induced convective snowbands over the Baltic Sea and their precipitation distribution. *Wea. Forecasting*, **5**, 299–312, doi:10.1175/1520-0434(1990)005<0299:TICSOT>2.0.CO;2.

Bech, J., N. Pineda, T. Rigo, and M. Aran, 2013: Remote sensing analysis of a Mediterranean thundersnow and low-altitude heavy snowfall event. *Atmos. Res.*, **123**, 305–322, doi:10.1016/j.atmosres.2012.06.021.

Behrangi, A., G. Stephens, R. F. Adler, G. J. Huffman, B. Lambrigtsen, and M. Lebsock, 2014: An update on the oceanic precipitation rate and its zonal distribution in light of advanced observations from space. *J. Climate*, **27**, 3957–3965, doi:10.1175/JCLI-D-13-00679.1.

Bintanja, R., and F. M. Selten, 2014: Future increases in Arctic precipitation linked to local evaporation and sea-ice retreat. *Nature*, **509**, 479–482, doi:10.1038/nature13259.

Boening, C., M. Lebsock, F. Landerer, and G. Stephens, 2012: Snowfall-driven mass change on the East Antarctic ice sheet. *Geophys. Res. Lett.*, **39**, L21501, doi:10.1029/2012GL053316.

Burnett, A. W., M. E. Kirby, H. T. Mullins, and W. P. Patterson, 2003: Increasing Great Lake–effect snowfall during the twentieth century: A regional response to global warming? *J. Climate*, **16**, 3535–3542, doi:10.1175/1520-0442(2003)016<3535:IGLSDT>2.0.CO;2.

Castellani, B. B., M. D. Shupe, D. R. Hudak, and B. E. Sheppard, 2015: The annual cycle of snowfall at Summit, Greenland. *J. Geophys. Res. Atmos.*, **120**, 6654–6668, doi:10.1002/2015JD023072.

Changnon, S. A., Jr., 1979: How a severe winter impacts on individuals. *Bull. Amer. Meteor. Soc.*, **60**, 110–114, doi:10.1175/1520-0477(1979)060<0110:HASWIO>2.0.CO;2.

Ellis, T. D., T. L'Ecuyer, J. M. Haynes, and G. L. Stephens, 2009: How often does it rain over the global oceans? The perspective from *CloudSat*. *Geophys. Res. Lett.*, **36**, L03815, doi:10.1029/2008GL036728.

Geerts, B., Y. Yang, R. Rasmussen, S. Haimov, and B. Pokharel, 2015: Snow growth and transport patterns in orographic storms as estimated from airborne vertical-plane dual-Doppler radar data. *Mon. Wea. Rev.*, **143**, 644–665, doi:10.1175/MWR-D-14-00199.1.

Hanna, E., J. McConnell, S. Das, J. Cappelen, and A. Stephens, 2006: Observed and modeled Greenland ice sheet snow

accumulation, 1958–2003, and links with regional climate forcing. *J. Climate*, **19**, 344–358, doi:10.1175/JCLI3615.1.

Haynes, J. M., T. S. L'Ecuyer, G. L. Stephens, S. D. Miller, C. Mitrescu, N. B. Wood, and S. Tanelli, 2009: Rainfall retrieval over the ocean with spaceborne W-band radar. *J. Geophys. Res.*, **114**, D00A22, doi:10.1029/2008JD009973.

——, ——, D. Vane, G. L. Stephens, and D. Reinke, 2013: Level 2-C precipitation column algorithm product process description and interface control document. Version P2_R04, *CloudSat* Project Doc., 17 pp. [Available online at http://www.cloudsat.cira.colostate.edu/sites/default/files/products/files/2C-PRECIP-COLUMN_PDICD.P2_R04.20130124.pdf.]

Henne, P. D., F. S. Hu, and D. T. Cleland, 2007: Lake-effect snow as the dominant control of mesic-forest distribution in Michigan, USA. *J. Ecol.*, **95**, 517–529, doi:10.1111/j.1365-2745.2007.01220.x.

Hiley, M. J., M. S. Kulie, and R. Bennartz, 2011: Uncertainty analysis for *CloudSat* snowfall retrievals. *J. Appl. Meteor. Climatol.*, **50**, 399–418, doi:10.1175/2010JAMC2505.1.

Holroyd, E. W., III, 1971: Lake-effect cloud bands as seen from weather satellites. *J. Atmos. Sci.*, **28**, 1165–1170, doi:10.1175/1520-0469(1971)028<1165:LECBAS>2.0.CO;2.

Hou, A. Y., and Coauthors, 2014: The Global Precipitation Measurement (GPM) mission. *Bull. Amer. Meteor. Soc.*, **95**, 701–722, doi:10.1175/BAMS-D-13-00164.1.

Hudak, D., P. Rodriguez, and N. Donaldson, 2008: Validation of the *CloudSat* precipitation occurrence algorithm using the Canadian C band radar network. *J. Geophys. Res.*, **113**, D00A07, doi:10.1029/2008JD009992.

Huffman, G. J., R. F. Adler, M. M. Morrissey, D. T. Bolvin, S. Curtis, R. Joyce, B. McGavock, and J. Susskind, 2001: Global precipitation at one-degree daily resolution from multisatellite observations. *J. Hydrometeor.*, **2**, 36–50, doi:10.1175/1525-7541(2001)002<0036:GPAODD>2.0.CO;2.

——, and Coauthors, 2007: The TRMM Multisatellite Precipitation Analysis (TMPA): Quasi-global, multiyear, combined-sensor precipitation estimates at fine scales. *J. Hydrometeor.*, **8**, 38–55, doi:10.1175/JHM560.1.

——, R. F. Adler, D. T. Bolvin, and G. Gu, 2009: Improving the global precipitation record: GPCP version 2.1. *Geophys. Res. Lett.*, **36**, L17808, doi:10.1029/2009GL040000.

Katsumata, M., H. Uyeda, K. Iwanami, and G. Liu, 2000: The response of 36- and 89-GHz microwave channels to convective snow clouds over ocean: Observation and modeling. *J. Appl. Meteor.*, **39**, 2322–2335, doi:10.1175/1520-0450(2000)039<2322:TROAGM>2.0.CO;2.

Kristovich, D. A. R., and R. Steve, 1995: A satellite study of cloud-band frequencies over the Great Lakes. *J. Appl. Meteor.*, **34**, 2083–2090, doi:10.1175/1520-0450(1995)034<2083:ASSOCB>2.0.CO;2.

——, and N. F. Laird, 1998: Observations of widespread lake-effect cloudiness: Influences of lake surface temperature and upwind conditions. *Wea. Forecasting*, **13**, 811–821, doi:10.1175/1520-0434(1998)013<0811:OOWLEC>2.0.CO;2.

Kneifel, S., M. Maahn, G. Peters, and C. Simmer, 2011: Observation of snowfall with a low-power FM-CW K-band radar (Micro Rain Radar). *Meteor. Atmos. Phys.*, **113**, 75–87, doi:10.1007/s00703-011-0142-z.

Kocin, P. J., and L. W. Uccellini, 1990: *Snowstorms along the Northeastern Coast of the United States: 1955–1985*. *Meteor. Monogr.*, No 44, Amer. Meteor. Soc., 280 pp.

Kolka, R. K., C. P. Giardina, J. D. McClure, A. Mayer, and M. F. Jurgensen, 2010: Partitioning hydrologic contributions to an 'old-growth' riparian area in the Huron Mountains of Michigan, USA. *Ecohydrology*, **3**, 315–324, doi:10.1002/eco.112.

Kulie, M. S., and R. Bennartz, 2009: Utilizing spaceborne radars to retrieve dry snowfall. *J. Appl. Meteor. Climatol.*, **48**, 2564–2580, doi:10.1175/2009JAMC2193.1.

——, ——, T. J. Greenwald, Y. Chen, and F. Z. Weng, 2010: Uncertainties in microwave properties of frozen precipitation implications for remote sensing and data assimilation. *J. Atmos. Sci.*, **67**, 3471–3487, doi:10.1175/2010JAS3520.1.

Kummerow, C., W. Barnes, T. Kozu, J. Shiue, and J. Simpson, 1998: The Tropical Rainfall Measuring Mission (TRMM) sensor package. *J. Atmos. Oceanic Technol.*, **15**, 809–817, doi:10.1175/1520-0426(1998)015<0809:TTRMMT>2.0.CO;2.

——, D. L. Randel, M. S. Kulie, N.-Y. Wang, R. Ferraro, S. J. Munchak, and V. Petkovic, 2015: The evolution of the Goddard profiling algorithm to a fully parametric scheme. *J. Atmos. Oceanic Technol.*, **32**, 2265–2280, doi:10.1175/JTECH-D-15-0039.1.

Kunkel, K. E., N. E. Westcott, and D. A. R. Kristovich, 2002: Assessment of potential effects of climate change on heavy lake effect snowstorms near Lake Erie. *J. Great Lakes Res.*, **28**, 521–536, doi:10.1016/S0380-1330(02)70603-5.

——, L. Ensor, M. Palecki, D. Easterling, D. Robinson, K. G. Hubbard, and K. Redmond, 2009: A new look at lake-effect snowfall trends in the Laurentian Great Lakes using a temporally homogeneous data set. *J. Great Lakes Res.*, **35**, 23–29, doi:10.1016/j.jglr.2008.11.003.

Laird, N. F., R. Sobash, and N. Hodas, 2010: Climatological conditions of lake-effect precipitation events associated with the New York State Finger Lakes. *J. Appl. Meteor. Climatol*, **49**, 1052–1062, doi:10.1175/2010JAMC2312.1.

Lebsock, M. D., and T. S. L'Ecuyer, 2011: The retrieval of warm rain from *CloudSat*. *J. Geophys. Res.*, **116**, D20209, doi:10.1029/2011JD016076.

——, ——, and G. L. Stephens, 2011: Detecting the ratio of rain and cloud water in low-latitude shallow marine clouds. *J. Appl. Meteor. Climatol.*, **50**, 419–432, doi:10.1175/2010JAMC2494.1.

Liu, C., and E. J. Zipser, 2009: "Warm rain" in the tropics: Seasonal and regional distributions based on 9 yr of TRMM data. *J. Climate*, **22**, 767–779, doi:10.1175/2008JCLI2641.1.

Liu, G., 2008: Deriving snow cloud characteristics from *CloudSat* observations. *J. Geophys. Res.*, **113**, D00A09, doi:10.1029/2007JD009766.

——, and E.-K. Seo, 2013: Detecting snowfall over land by satellite high-frequency microwave observations: The lack of scattering signature and a statistical approach. *J. Geophys. Res. Atmos.*, **118**, 1376–1387, doi:10.1002/jgrd.50172.

Maahn, M., C. Burgard, S. Crewell, I. V. Gorodetskaya, S. Kneifel, S. Lhermitte, K. Van Tricht, and N. P. M. van Lipzig, 2014: How does the spaceborne radar blind zone affect derived surface snowfall statistics in polar regions? *J. Geophys. Res. Atmos.*, **119**, 13 2604–13 2620, doi:10.1002/2014JD022079.

Marchand, R., G. G. Mace, T. Ackerman, and G. Stephens, 2008: Hydrometeor detection using *Cloudsat*—An Earth-orbiting 94-GHz cloud radar. *J. Atmos. Oceanic Technol.*, **25**, 519–533, doi:10.1175/2007JTECHA1006.1.

Mazon, J., S. Niemelä, D. Pino, H. Savijärvi, and T. Vihma, 2015: Snow bands over the Gulf of Finland in wintertime. *Tellus*, **67A**, 25102, doi:10.3402/tellusa.v67.25102.

Matrosov, S. Y., 2007: Modeling backscatter properties of snowfall at millimeter wavelengths. *J. Atmos. Sci.*, **64**, 1727–1736, doi:10.1175/JAS3904.1.

——, M. D. Shupe, and I. V. Djalalova, 2008: Snowfall retrievals using millimeter-wavelength cloud radars. *J. Appl. Meteor. Climatol*, **47**, 769–777, doi:10.1175/2007JAMC1768.1.

Milani, L., F. Porcù, D. Casella, S. Dietrich, G. Panegrossi, M. Petracca, and P. Sanò, 2015: Analysis of long-term precipitation pattern over Antarctica derived from satellite-borne radar. *Cryosphere Discuss.*, **9**, 141–182, doi:10.5194/tcd-9-141-2015.

Niziol, T. A., 1987: Operational forecasting of lake effect snowfall in western and central New York. *Wea. Forecasting*, **2**, 310–321, doi:10.1175/1520-0434(1987)002<0310:OFOLES>2.0.CO;2.

Noh, Y.-J., G. Liu, E.-K. Seo, J. R. Wang, and K. Aonashi, 2006: Development of a snowfall retrieval algorithm at high microwave frequencies. *J. Geophys. Res.*, **111**, D22216, doi:10.1029/2005JD006826.

Norris, J., G. Vaughan, and D. M. Schultz, 2013: Snowbands over the English Channel and Irish Sea during cold-air outbreaks. *Quart. J. Roy. Meteor. Soc.*, **139**, 1747–1761, doi:10.1002/qj.2079.

Norton, D. C., and S. J. Bolsenga, 1993: Spatiotemporal trends in lake effect and continental snowfall in the Laurentian Great Lakes, 1951–1980. *J. Climate*, **6**, 1943–1955, doi:10.1175/1520-0442(1993)006<1943:STILEA>2.0.CO;2.

Notaro, M., K. Holman, A. Zarrin, E. Fluck, S. Vavrus, and V. Bennington, 2013: Influence of the Laurentian Great Lakes on regional climate. *J. Climate*, **26**, 789–804, doi:10.1175/JCLI-D-12-00140.1.

——, D. Lorenz, C. Hoving, and M. Schummer, 2014: Twenty-first-century projections of snowfall and winter severity across central-eastern North America. *J. Climate*, **27**, 6526–6550, doi:10.1175/JCLI-D-13-00520.1.

Palerme, C., J. E. Kay, C. Genthon, T. L'Ecuyer, N. B. Wood, and C. Claud, 2014: How much snow falls on the Antarctic ice sheet? *Cryosphere*, **8**, 1577–1587, doi:10.5194/tc-8-1577-2014.

Plummer, D. M., G. M. McFarquhar, R. M. Rauber, B. F. Jewett, and D. C. Leon, 2014: Structure and statistical analysis of the microphysical properties of generating cells in the comma head region of continental winter cyclones. *J. Atmos. Sci.*, **71**, 4181–4203, doi:10.1175/JAS-D-14-0100.1.

Pokharel, B., B. Geerts, X. Jing, K. Friedrich, J. Aikins, D. Breed, R. Rasmussen, and A. Huggins, 2014: The impact of ground-based glaciogenic seeding on clouds and precipitation over mountains: A multi-sensor case study of shallow precipitating orographic cumuli. *Atmos. Res.*, **147–148**, 162–182, doi:10.1016/j.atmosres.2014.05.014.

Rauber, R. M., and Coauthors, 2014: Stability and charging characteristics of the comma head region of continental winter cyclones. *J. Atmos. Sci.*, **71**, 1559–1582, doi:10.1175/JAS-D-13-0253.1.

Rapp, A. D., M. Lebsock, and T. L'Ecuyer, 2013: Low cloud precipitation climatology in the southeastern Pacific marine stratocumulus region using *CloudSat*. *Environ. Res. Lett.*, **8**, 014027, doi:10.1088/1748-9326/8/1/014027.

Sassen, K., and Z. Wang, 2008: Classifying clouds around the globe with the *CloudSat* radar: 1-year of results. *Geophys. Res. Lett.*, **35**, L04805, doi:10.1029/2007GL032591.

Schmidlin, T. W., 1993: Impacts on severe winter weather during December 1989 in the Lake Erie snowbelt. *J. Climate*, **6**, 759–767, doi:10.1175/1520-0442(1993)006<0759:IOSWWD>2.0.CO;2.

——, D. J. Edgell, and M. A. Delaney, 1992: Design ground snow loads for Ohio. *J. Appl. Meteor.*, **31**, 622–627, doi:10.1175/1520-0450(1992)031<0622:DGSLFO>2.0.CO;2.

Schultz, D. M., 1999: Lake-effect snowstorms in northern Utah and western New York with and without lightning. *Wea. Forecasting*, **14**, 1023–1031, doi:10.1175/1520-0434(1999)014<1023:LESINU>2.0.CO;2.

Schumacher, C., and R. A. Houze, 2003: The TRMM Precipitation Radar's view of shallow, isolated rain. *J. Appl. Meteor.*, **42**, 1519–1524, doi:10.1175/1520-0450(2003)042<1519:TTPRVO>2.0.CO;2.

Scott, R. W., and F. A. Huff, 1996: Impacts of the Great Lakes on regional climate conditions. *J. Great Lakes Res.*, **22**, 845–863, doi:10.1016/S0380-1330(96)71006-7.

Shepherd, A., and Coauthors, 2012: A reconciled estimate of ice-sheet mass balance. *Science*, **338**, 1183–1189, doi:10.1126/science.1228102.

Short, D. A., and K. Nakamura, 2000: TRMM radar observations of shallow precipitation over the tropical oceans. *J. Climate*, **13**, 4107–4124, doi:10.1175/1520-0442(2000)013<4107:TROOSP>2.0.CO;2.

Shupe, M. D., S. Y. Matrosov, and T. Uttal, 2006: Arctic mixed-phase cloud properties derived from surface-based sensors at SHEBA. *J. Atmos. Sci.*, **63**, 697–711, doi:10.1175/JAS3659.1.

——, and Coauthors, 2013: High and dry: New observations of tropospheric and cloud properties above the Greenland Ice Sheet. *Bull. Amer. Meteor. Soc.*, **94**, 169–186, doi:10.1175/BAMS-D-11-00249.1.

Simpson, J., R. F. Adler, and G. R. North, 1988: A proposed Tropical Rainfall Measuring Mission (TRMM) satellite. *Bull. Amer. Meteor. Soc.*, **69**, 278–295, doi:10.1175/1520-0477(1988)069<0278:APTRMM>2.0.CO;2.

Steenburgh, W. J., S. F. Halvorson, and D. J. Onton, 2000: Climatology of lake-effect snowstorms of the Great Salt Lake. *Mon. Wea Rev.*, **128**, 709–727, doi:10.1175/1520-0493(2000)128<0709:COLESO>2.0.CO;2.

Stephens, G. L., and Coauthors, 2002: The *CloudSat* mission and the A-Train. *Bull. Amer. Meteor. Soc.*, **83**, 1771–1790, doi:10.1175/BAMS-83-12-1771.

Tanelli, S., S. L. Durden, E. Im, K. S. Pak, D. G. Reinke, P. Partain, J. M. Haynes, and R. T. Marchand, 2008: *CloudSat*'s Cloud Profiling Radar after two years in orbit: Performance, calibration, and processing. *IEEE Trans. Geosci. Remote Sens.*, **46**, 3560–3573, doi:10.1109/TGRS.2008.2002030.

Thomas, B. C., and J. E. Martin, 2007: A synoptic climatology and composite analysis of the Alberta Clipper. *Wea. Forecasting*, **22**, 315–333, doi:10.1175/WAF982.1.

Wang, Y., G. Liu, E.-K. Seo, and Y. Fu, 2013: Liquid water in snowing clouds: Implications for satellite remote sensing of snowfall. *Atmos. Res.*, **131**, 60–72, doi:10.1016/j.atmosres.2012.06.008.

Wang, Z., and K. Sassen, 2007: Level 2 cloud scenario classification product process description and interface control document. Version 5.0, *CloudSat* Project Doc., 50 pp. [Available online at http://www.cloudsat.cira.colostate.edu/sites/default/files/products/files/2B-CLDCLASS_PDICD.P_R04.20070724.pdf.]

Wood, N. B., T. S. L'Ecuyer, D. Vane, G. L. Stephens, and P. Partain, 2013: Level 2C snow profile process description and interface control document. JPL Doc., 21 pp.

——, ——, A. J. Heymsfield, G. L. Stephens, D. R. Hudak, and P. Rodriguez, 2014: Estimating snow microphysical properties using collocated multisensor observations. *J. Geophys. Res. Atmos.*, **119**, 8941–8961, doi:10.1002/2013JD021303.

——, ——, ——, and ——, 2015: Microphysical constraints on millimeter-wavelength scattering properties of snow particles. *J. Appl. Meteor. Climatol.*, **54**, 909–931, doi:10.1175/JAMC-D-14-0137.1.

Yeager, K. N., W. J. Steenburgh, and T. I. Alcott, 2013: Contributions of lake-effect periods to the cool-season hydroclimate of the Great Salt Lake basin. *J. Appl. Meteor. Climatol.*, **52**, 341–362, doi:10.1175/JAMC-D-12-077.1.